

Article

Controlled Excitation of Supermodes in a Multicore Fiber with a 5×5 Square Array of Strongly Coupled Cores

Nikolay A. Kalinin ¹, Elena A. Anashkina ¹ , Olga N. Egorova ², Sergey G. Zhuravlev ³, Sergei L. Semjonov ³, Arkady V. Kim ¹, Alexander G. Litvak ¹ and Alexey V. Andrianov ^{1,*}

¹ Institute of Applied Physics of the Russian Academy of Sciences, 603950 Nizhny Novgorod, Russia; nkalinin@ipfran.ru (N.A.K.); elena.anashkina@ipfran.ru (E.A.A.); kim@ufp.appl.sci-nnov.ru (A.V.K.); litvak@appl.sci-nnov.ru (A.G.L.)

² Prokhorov General Physics Institute of the Russian Academy of Sciences, 119991 Moscow, Russia; egorova@nsc.gpi.ru

³ Dianov Fiber Optics Research Center, Prokhorov General Physics Institute of the Russian Academy of Sciences, 119991 Moscow, Russia; mazerator3000@yandex.ru (S.G.Z.); sls@fo.gpi.ru (S.L.S.)

* Correspondence: andrian@ipfran.ru

Abstract: Coherent propagation of supermodes in a multicore fiber is promising for power scaling of fiber laser systems, eliminating the need for the active feedback system to maintain the phases between the channels. We studied the propagation of broadband pulsed radiation at a central wavelength of 1030 nm in a multicore fiber with coupled cores arranged in a square array. We designed and fabricated a silica multicore fiber with a 5×5 array of cores. For controllable excitation of a desired supermode, we developed a beam-forming system based on a spatial light modulator. We experimentally measured intensity and phase distributions of the supermodes, in particular, the in-phase and out-of-phase supermodes, which matched well the numerically calculated profiles. We obtained selective excitation and coherent propagation of broadband radiation with the content of the out-of-phase supermode of up to 90% maintained without active feedback. Using three-dimensional numerical modeling with allowance for a refractive index profile similar to those of the developed fiber, we demonstrated stable propagation of the out-of-phase supermode and collapse of the in-phase supermode at a high signal power.

Keywords: multicore fiber; supermode; nonlinear light propagation; spatial light modulator



Citation: Kalinin, N.A.; Anashkina, E.A.; Egorova, O.N.; Zhuravlev, S.G.; Semjonov, S.L.; Kim, A.V.; Litvak, A.G.; Andrianov, A.V. Controlled Excitation of Supermodes in a Multicore Fiber with a 5×5 Square Array of Strongly Coupled Cores. *Photonics* **2021**, *8*, 314. <https://doi.org/10.3390/photonics8080314>

Received: 6 July 2021

Accepted: 30 July 2021

Published: 4 August 2021

Publisher's Note: MDPI stays neutral with regard to jurisdictional claims in published maps and institutional affiliations.



Copyright: © 2021 by the authors. Licensee MDPI, Basel, Switzerland. This article is an open access article distributed under the terms and conditions of the Creative Commons Attribution (CC BY) license (<https://creativecommons.org/licenses/by/4.0/>).

1. Introduction

The spatial degree of freedom has recently attracted much attention in fiber optics for increasing the capacity of fiber links [1] and increasing the optical power of laser systems. Spatial multiplexing for high-bit-rate data transmission in multimode fibers was proposed [2] and demonstrated in various fibers [3], including active fibers [4] (see also [1] and references therein). In high-power laser systems, multimode fibers are used to reduce nonlinearity, however, to attain good beam quality, single-mode propagation is desirable, which can be achieved in several fiber designs: step-index fibers with a microstructured cladding for suppressing high-order modes [5], leakage channel fibers [6], helical-core fibers [7], chirally coupled core fibers [8], photonic bandgap fibers [9], and fibers intentionally operated in high-order mode [10]. Multicore fibers (MCF) are promising for coherent transportation and amplification of high average and peak power signals. Active and passive multicore fibers with weakly interacting cores are actively studied in the context of high-speed telecommunications [11–14], including quantum key distribution [15,16], high-power beam delivery and amplification [17–19], as well as synthesis of complex beam structures by coherent combining of the MCF output radiation [20]. However, in order to coherently combine light from noninteracting cores, an active feedback system is required to compensate for phase fluctuations in different cores [17,18]. In contrast, multicore fibers

with sufficiently coupled cores [21] support the propagation of the supermodes in which the coherency between the light in the cores can be maintained without the need for any feedback system. Moreover, the MCFs with coupled cores are attractive for exploration of many nonlinear and laser phenomena, including selective mode amplification [22], Raman lasing [23,24], spatiotemporal pulse compression [25,26], light bullet and soliton formation [27–29], supercontinuum generation [30], radiation trapping, and pulse cleaning [31,32]. Recent studies have shown that in the MCFs with coupled cores there are regimes of light propagation that are stable at high power and maintain coherency between the channels [33–36]. Such regimes are promising for designing novel high-power laser systems.

It was predicted theoretically [33–37] and then shown in an experiment that in the MCFs with N cores arranged in a ring close to each other, the light with transversal structure of the out-of-phase supermode can propagate and be amplified [38]. In this supermode the intensity is equal in all cores, whereas the phase of the light in neighboring cores differs by π . This structure is stable with respect to different fluctuations and does not suffer from discrete self-focusing [39] up to the peak power N times greater than the self-focusing limit in a single-core fiber [33]. Unfortunately, the size of such MCFs grows fast with increasing number of cores, and it becomes difficult to fabricate them.

Better scaling of the number of cores with the linear size of the fiber is achieved in MCFs with a square array of cores. Recently, it was predicted theoretically and numerically that with such an arrangement of cores there exists an out-of-phase supermode, too, where the light phase in the cores is 0 and π following the chessboard pattern [36]. It was shown theoretically that, in principle, the power carried in this mode can be N times higher than the limiting power of a single core. According to the theory, the intensity distribution is nonuniform at low powers (it is higher in the central core and lower at the peripheral), however, it equalizes with increasing power [36]. Besides, it was shown in a recent work [40] that radiation with a transverse structure of such a supermode can be easily coherently combined with high efficiency. Until now, to the best of our knowledge, active and passive MCFs with a square array of uncoupled cores have only been studied in terms of spatial-multiplexed data transfer [41–43], optical amplification [18,44], and demonstration of coherent combining using an in-phase pattern [19]. The possibility of selective supermode excitation in an MCF with a square array of coupled cores, in particular, the out-of-phase supermode (the most interesting for power scaling), has not been studied in experiment.

In the presented work, we fabricated a silica MCF with 25 cores arranged close to each other in a 5×5 square lattice. The individual cores were single-mode at the operating wavelength of 1030 nm and were placed close enough to provide sufficient coupling. We demonstrated the possibility of selective excitation and coherent propagation of broadband radiation in this MCF with a transverse structure corresponding to the MCF supermodes. For the first time, to our knowledge, we demonstrated the excitation and propagation of the out-of-phase supermode in an MCF with a square array of cores. We developed an experimental setup that allows changing the content of different supermodes in the signal, in particular, selectively exciting a certain supermode. We showed the possibility of selective excitation of the out-of-phase supermode so that it contains 90% of the power at the output of the MCF. Using three-dimensional numerical modeling with allowance for the real geometrical structure of the MCF cores, we demonstrated stability of the out-of-phase supermode at high power levels.

The remainder of the manuscript is structured as follows. In Section 2, we briefly review some important facts from the theory of light propagation in MCFs with a square array of cores. In Section 3, we provide the information about the MCF fabrication technology and the geometry of the MCF. In Section 4, we show the results of a numerical computation of supermodes and their properties in the fabricated MCF. In Section 5, we describe the experimental setup for studying the light propagation in the MCF and demonstrate the obtained results. In Section 6, we demonstrate the results of numerical simulation

of high-power light propagation in our MCF. In Section 7, we discuss the next steps in studying MCFs of similar design. Finally, we summarize the obtained results in Section 8.

2. Theoretical Background

In this section, we recall the theoretical background of light propagation in MCFs, paying special attention to the stability of high-power light propagation. In an MCF with single-mode cores, the light propagation can be described by a discrete set of one-dimensional nonlinear coupled Schrödinger equations. For a square array of $N \times N$ cores with allowance for coupling of each core with its four nearest neighbors, we obtain [36]

$$i \frac{\partial a_{nm}}{\partial z} + \chi(a_{n-1,m} + a_{n+1,m} + a_{n,m-1} + a_{n,m+1}) + \gamma a_{nm} |a_{nm}|^2 = 0. \tag{1}$$

Here, a_{nm} is the field amplitude in (n, m) core, $n, m = 1 \dots N$, $\chi > 0$ is the coupling coefficient, and $\gamma > 0$ is the nonlinear coefficient. The boundary conditions for a square $N \times N$ array of cores can be easily formulated by adding virtual rows of cores at the boundaries ($n = N + 1, n = 0, m = N + 1, m = 0$) and setting zero amplitudes in these cores. We note that coupled nonlinear Schrödinger equations are widely used to describe various nonlinear phenomena, including solitons and breathers, in arrays of optically and optomechanically coupled devices [45,46]. At low nonlinearity ($\gamma a \ll 1$), the standard procedure of finding eigen solutions of Equation (1) results in N^2 supermodes. Two supermodes—the lowest one having the same phases in all cores (in-phase supermode) and the highest one having 0 and π phases following the chessboard pattern (out-of-phase supermode)—are important for our study. It is known that at high powers the in-phase supermode is subject to discrete modulation instability. However, the out-of-phase supermode is stable at high powers up to the limit of self-focusing in each core [36]. The origin of this effect can be easily illustrated for large arrays. Using the ansatz

$$a_{nm} = g(n, m)(-1)^{n+m} \tag{2}$$

and assuming smoothness of the function $g(n, m)$ we can approximate the discrete coupling terms in Equation (1) by continuous derivatives and obtain.

$$i \frac{\partial g(n, m)}{\partial z} - \chi \left(\frac{\partial^2 g(n, m)}{\partial n^2} + \frac{\partial^2 g(n, m)}{\partial m^2} \right) + \gamma g |g|^2 = 0. \tag{3}$$

This equation resembles the equation describing nonlinear diffraction in a homogeneous medium, with an important difference in the sign of the diffraction term. This combination of diffraction and nonlinearity leads to defocusing dynamics; hence, the system is not subject to the transverse modulation instability. At low power ($\gamma |g|^2 \ll 1$), the mode envelope can be approximated by the lowest mode of a rectangular waveguide:

$$g \propto \sin\left(\frac{\pi n}{N+1}\right) \sin\left(\frac{\pi m}{N+1}\right). \tag{4}$$

In a nonlinear regime, the mode envelope cannot be found analytically, but the numerical modeling shows that with increasing power the profile becomes flatter so that the light is redistributed more evenly over all the cores. We introduce new variables $X = n/(N + 1)$, $Y = m/(N + 1)$, $Z = z\chi/(N + 1)^2$, and $G = g(N + 1)\sqrt{\gamma/\chi}$ and rewrite Equation (3) in dimensionless form

$$i \frac{\partial G(X, Y)}{\partial Z} - \frac{\partial^2 G(X, Y)}{\partial X^2} - \frac{\partial^2 G(X, Y)}{\partial Y^2} + G|G|^2 = 0. \tag{5}$$

For all N , the zero boundary conditions are now set at $X, Y = 0$ and $X, Y = 1$. The numerical modeling of the rescaled equation shows that the profile of the out-of-phase supermode becomes more or less flat (the amplitude is above 0.8 of its maximum for

80% of the total area) at the peak amplitude $G_p \sim 20$. Returning to the dimensional variables, we obtain the scaling law for the peak power required to equalize the out-of-phase mode profile:

$$|a|^2 \sim \frac{\chi G_p^2}{\gamma(N+1)^2}. \quad (6)$$

To transport signals with large peak power, the nonlinear coefficient should be kept small, although it is not easy to decrease γ significantly. Typical values for all-solid silica fibers are of the order of $1/W/\text{km}$. It is noteworthy that achieving mode profile equalization is easier for the fiber with large number of cores; however, the total power combined in all cores proportional to $|a|^2 N^2$ remains the same. The coupling coefficient can be varied in a broad range by adjusting the core-to-core distance. This can be used to adjust the MCF properties for the required signal power. Great care should be taken if low coupling coefficients are chosen. Although the out-of-phase supermode is stable against perturbations, such as fiber bending and gain in active fibers [35], the characteristic length at which the supermode adjusts its properties to compensate for the perturbation is proportional to the effective coupling length $1/\chi$ and must be short enough. Bearing the above considerations in mind, we designed and fabricated an MCF with a 5×5 array of sufficiently coupled cores.

3. MCF Fabrication

For maintaining stable supermode propagation, especially in the presence of imperfections and high nonlinearity, the cores must be coupled well enough [36]. For this, the modes of neighboring cores should overlap significantly. Besides, each individual core should be single-mode at the working wavelengths. These two factors require the distance between the cores in the MCF and the refractive index difference of each core to be small, therefore, it is not easy to assemble such an MCF using several standard single-core preforms or homogeneous rods. We used a two-step process, shown schematically in Figure 1, to fabricate our MCF. At the first step, we assembled a preform for individual cores with a large cladding-to-core diameter ratio using a large number of silica rods with smaller Ge-doped cores inserted into a thin-walled silica tube (see Figure 1a). When the preform was drawn, the typical scale of this structure became much smaller than the wavelength, and thus we were able to form the required effective refractive index for the individual cores. The diameter of the core in this single-core preform was about 0.7 of the diameter of the cladding. At the second step, we used these single-core preforms to assemble a multicore preform (Figure 1b). The assembled preform was then consolidated and a fiber of the required diameter was drawn. The image of the manufactured MCF's end face is shown in Figure 1c. The cladding diameter of the MCF is $200 \mu\text{m}$, the core-to-core distance is about $8.4 \mu\text{m}$, and the diameter of the cores is about $6 \mu\text{m}$. The refractive index difference is about 0.005, and the numerical aperture of the individual core is $\text{NA} \sim 0.12$. The optical losses estimated using relatively short (a few tens of meters) fiber pieces are $<10 \text{ dB/km}$.

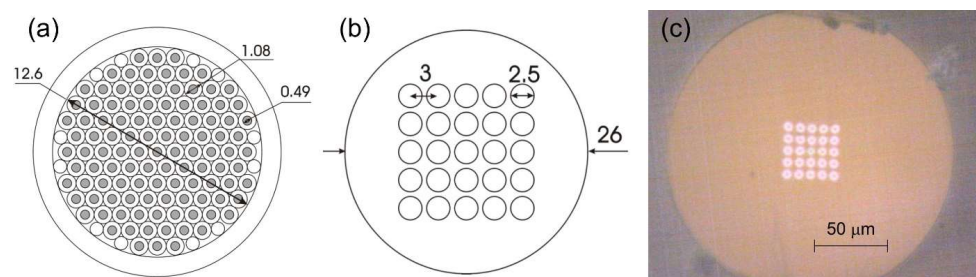


Figure 1. Fabrication of the MCF: (a) preform for individual core, (b) multicore preform, (c) microphotography of the manufactured MCF. Dimensions in (a,b) are given in mm.

4. Supermodes in the Fabricated MCF

Using the transversal structure of the refractive index in the fabricated MCF, we calculated the supermodes, their effective refractive indexes, and group velocities. We used the finite-element model in the COMSOL package for these computations. The central wavelength was assumed to be 1030 nm; each individual core is single-mode at this wavelength. The refractive index profiles in the cores were approximated by step-profiles with the sizes shown in the inset in Figure 2.

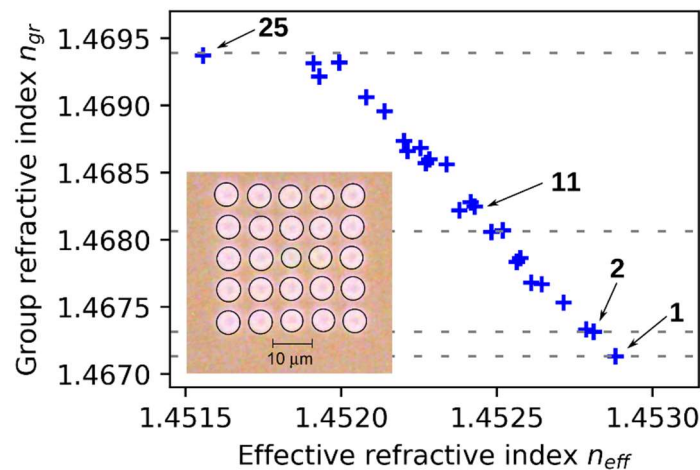


Figure 2. Numerically calculated (blue crosses) effective refractive indexes and group indexes of supermodes of the fabricated MCF. Group indexes of the 1st, 2nd, 11th, and 25th supermodes (grey dashed lines) measured in the experimental scheme shown in Figure 3. The numbers mark the 1st (in-phase), 2nd, 11th, and 25th (out-of-phase) supermodes shown in Figure 4. Experimentally measured (grey dashed lines) group indexes of the 1st, 2nd, 11th, and 25th supermodes. The inset shows the size and location of cores in the MCF used for modeling.

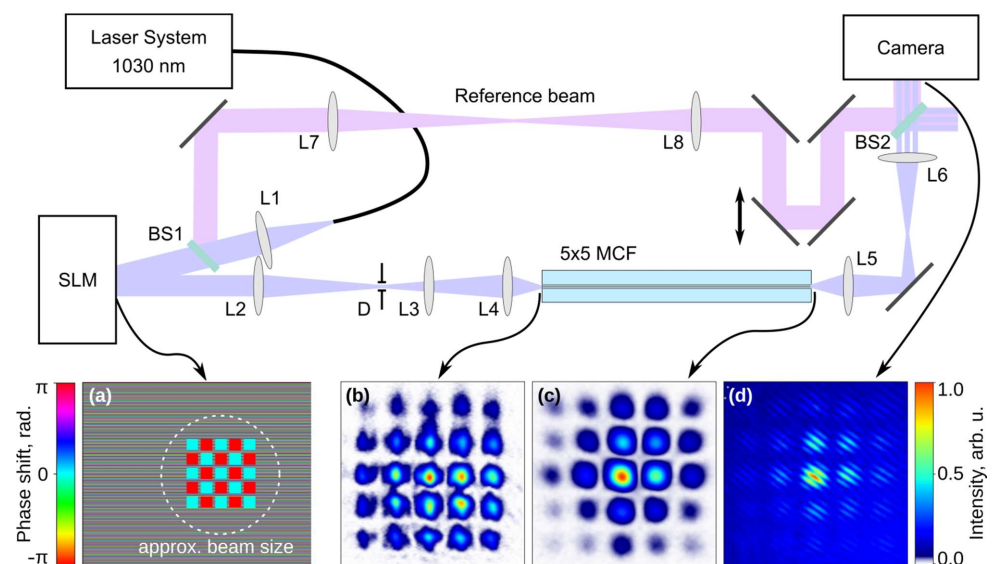


Figure 3. Schematic of experimental setup for studying supermodes propagation in MCF. L1–L8—lenses; D—a diaphragm; BS1, BS2—50/50 beamsplitters. Insets: (a) phase mask on the SLM; (b) intensity distribution image at the input face of the MCF; (c) intensity distribution image at the output face of the MCF; (d) interference picture when group delays of the reference beam and the out-of-phase supermode are matched. All insets correspond to the out-of-phase supermode excitation.

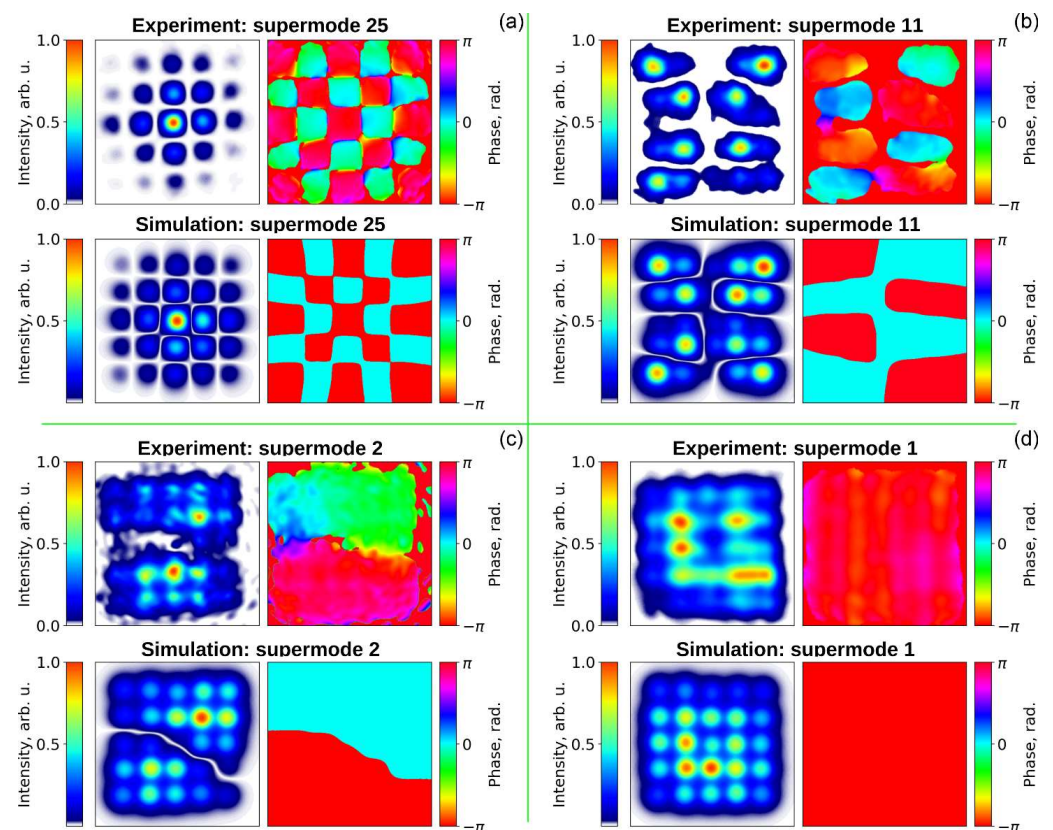


Figure 4. Measured (upper panels in each subplot) and numerically calculated (**lower panels**) intensity (**left panels**) and phase (**right panels**) distributions of supermodes 25 (out-of-phase; (a)), 11 (b), 2 (c), and 1 (in-phase; (d)).

In the case of a perfect MCF structure, there are a total of 25 supermodes (50 considering the polarization degeneracy); most of them are degenerate due to the structure symmetry. The degeneracy is removed for the nonideal structure of the fabricated MCF, however, there are groups of modes with close parameters. The calculated effective refractive indexes and group indexes are shown in Figure 2. The magnitude and phase profiles of several supermodes, including the in-phase and the out-of-phase supermodes (calculated and measured according to our experimental scheme depicted in Figure 3, see detailed discussion below), are shown in Figure 4. We estimated the beat length between neighboring cores to be 2.7 mm, confirming relatively strong coupling. We could also see significant overlapping of neighboring core modes on the magnitude profiles. Strong coupling of the cores and a small beat length are required for stable propagation considering manufacturing errors in the strongly nonlinear regime.

5. Experimental Study of Supermodes Propagation in MCF

We studied the possibility of selective excitation of supermodes in the fabricated MCF using a low-power laser source. The experimental setup for studying light propagation in the fabricated MCF is shown in Figure 3. The radiation source was a homemade laser system consisting of a master laser [47], a fiber stretcher, and a two-stage ytterbium amplifier [48]. The system generated 50-ps chirped pulses at a central wavelength of 1030 nm with a spectral width corresponding to a Fourier-transform-limited duration of ~ 220 fs. A specially designed scheme was developed to deliver the pulses to the MCF.

We used a liquid crystal spatial phase light modulator (SLM, Hamamatsu, 1024×1200 pixels) to form the required spatial beam pattern at the input face of the MCF. The radiation outcoming from the seed system was collimated using lens L1 (focal length 40 mm) and directed to the SLM, where it had an almost flat phase distribution. Then we introduced

the required phase shift at each transversal point of the reflected beam using the SLM and imaged the SLM plane to the input face of the fiber using a three-lens telescope (lenses L2, L3, and L4 with focal lengths 200 mm, 40 mm, and 6.24 mm, respectively). The telescope produced $98.6\times$ demagnification. In order to form the intensity modulation, we discarded some parts of the input beam by creating a strong phase gradient and filtering out these parts with the diaphragm D installed in the Fourier plane of the telescope. In our scheme, the required beam profile was synthesized in the near field with respect to the SLM, contrary to the often-used approach in which the required profile was formed in the far field [17,38]. The near-field approach allows a more precise control of the amplitude and phase in the forming beamlets when the number of beamlets is large. To excite supermodes in the MCF, we formed a beam consisting of 25 square beamlets arranged in a 5×5 array. The required phase mask for the SLM and the intensity distribution of the synthesized beam (imaged with a $60 \times$ magnification lens by an auxiliary telescope) are shown in the insets in Figure 3a,b. We can see 25 beamlets in a 5×5 array. The central beamlets had a higher intensity because the intensity of the initial beam was higher in the center.

Each beamlet was directed to the corresponding core of the MCF. We detected the locations on the SLM image corresponding to each core of the MCF using the following approach. We switched off all the squares on the SLM except one, and then started moving this square on the SLM while measuring the coupling efficiency of the beam to the MCF. Afterward, we placed the squares on the SLM at the spots corresponding to the maximum coupling efficiency. The resulting scheme allowed us to couple the light with controlled intensity and phase to an arbitrary set of cores in the MCF. To change the phase of a single beamlet we had to change the phase of the corresponding square on the SLM, and to change the power in the beamlet we needed to change the size of the square (and thus the size of the beamlet itself).

The length of the used MCF was 0.67 m, which is much longer than the characteristic coupling length, so the supermodes formed at the very beginning of the fiber. For studying the output radiation from the MCF, the output face of the MCF was imaged with $60 \times$ magnification using lenses L5 and L6 onto a CCD camera. The intensity distribution at the output face of the MCF when the out-of-phase supermode was launched is shown in Figure 3c. To obtain intensity and phase profiles of individual supermodes, as well as to estimate the content of each excited supermode, we used an interference setup similar to the one we used in [38]. A reference beam with a flat spatial phase was split off the main beam before the SLM via beamsplitter BS1, then transmitted through lenses L7 and L8 and the adjustable delay line to the camera, recombining with the studied beam at the beamsplitter BS2 at a small angle. The supermodes in the MCF had different group velocities, so by adjusting the reference beam delay line we were able to match the group delay of the reference beam with the group delay of different supermodes. In each measurement, a set of interference pictures with different reference delays was recorded and processed. A strong interference pattern from a particular supermode was only visible when the difference between its group delay and the group delay of the reference beam was within the coherency time of the source laser system (250 fs). The difference between group delays of the highest (out-of-phase) and the lowest (in-phase) supermodes was about 4.8 ps in our case and allowed the supermodes to be distinguished. Confirming this, the peaks of visibility of the interference pattern were clearly visible when we were changing the reference delay. An example of an interference pattern with the reference group delay matching the out-of-phase mode group delay is shown in Figure 3d.

The intensity and phase distributions of supermodes were retrieved by Fourier filtering the interference image. The intensity and phase distributions of several supermodes, including the lowest (#1, in-phase), the highest (#25, out-of-phase), and two intermediate (#2, #11) supermodes are shown in Figure 4 along with numerically calculated profiles (the mode numbering is in the order of decreasing effective index values). We can see that the measured distributions match numerical predictions well. The input power in this experiment was 10 MW, corresponding to the pulse energy of 0.4 nJ and the peak

power of 7 W, so a linear propagation regime was realized. The retrieved mode profiles did not change with the variations of the input power, which was still too low to observe the nonlinear effects. The group delay of the in-phase supermode was the smallest, whereas the group delay of the out-of-phase supermode was the largest in a good agreement with the numerical calculations. Besides, the interference visibility maxima for particular supermodes were well separated from the others, indicating that there was no continuous energy transfer between the supermodes. Otherwise, the interference would be visible at any delay of the reference signal. The visibility amplitudes at different peaks were proportional to the content of the corresponding supermodes in the pulse. The group refractive index differences between four supermodes, shown in Figure 4, were retrieved. Taking the group index of the in-phase supermode as a reference, we plotted the retrieved group indexes in Figure 2. Measured values agree well with the calculated ones. Although we did not test longer fiber pieces, we believe that observed supermodes can propagate steadily in long fibers since we did not observe significant energy transfer between the modes. Note that our technology of MCF fabrication allows drawing of kilometer lengths of continuous fiber [49].

For a more detailed study of the supermode properties, and for transmitting high-power radiation through an MCF, the light must be coupled into a certain supermode without exciting the other supermodes. In order to ideally excite a single supermode the beam profile at the input face of the MCF must match the magnitude and phase profile of this supermode. It is difficult to form such a beam for several reasons, including the limitations of the system that synthesizes the beam, phase distortions by different optical elements, the angle of the fiber input face, and the fiber input face non-flatness. In our input system, the power and phase in each beamlet corresponding to a single core of the MCF can be changed independently, and this gives us enough degrees of freedom to minimize excitation of undesirable supermodes. In order to optimize the fraction of the power contained in a specific supermode, we changed the phase mask on the SLM, adjusting the power and phase in the 25 synthesized beamlets. We implemented a numerical algorithm based on a stochastic gradient descent to search the optimal phase mask. The algorithm used the supermodes content analysis system described above as the feedback source, calculating the content of the desired supermode after each change. The algorithm started from the equal powers in each beamlet; for the in-phase supermode, the algorithm chose a flat phase distribution, whereas for the out-of-phase supermode it started from opposite phases in the neighboring cores. To speed up the process, only two types of changes were applied at the first stage of the algorithm: a linear phase gradient common for all cores and a symmetrical decrease of beamlet sizes of the outer cores. At the second stage, the algorithm applied arbitrary changes to phases and sizes of each individual beamlet. After each change, the algorithm measured the content of the desired supermode and reverted the change if the content of the desired supermode did not increase.

We were primarily interested in the possibility of selective excitation of the out-of-phase supermode as the most promising one for transmitting high power. After optimization, 88% of the pulse power was contained in the out-of-phase supermode. This number is limited by the capabilities of the system that synthesizes the beam using the SLM. The beam outcoming from the output of the fiber when the out-of-phase supermode is selectively excited is shown in Figure 3c. We can see that it corresponds to the calculated intensity distribution of this supermode very well. The spectrum of the radiation from the MCF when the out-of-phase supermode is selectively excited is shown in Figure 5 in comparison with the spectrum of the seed source. We can see small-amplitude interference fringes in the spectrum, indicating the presence of more than one supermode in the signal. However, the small amplitude of the interference proves that the desired supermode contains much more power than the other modes. Apart from small modulation, the spectrum coincides with the seed spectrum.

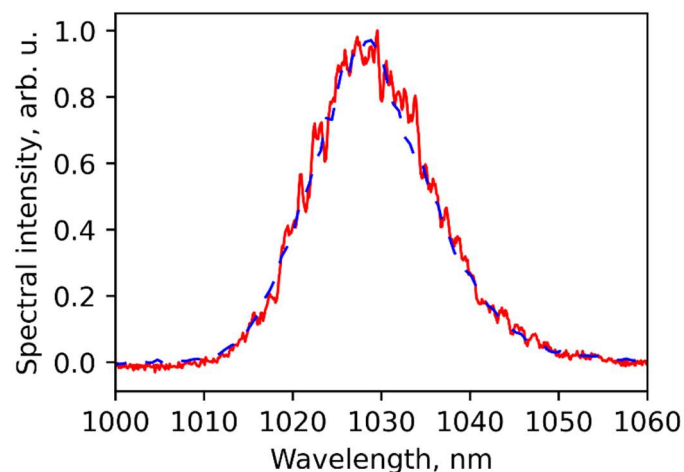


Figure 5. Spectrum of radiation passed through the MCF when the out-of-phase supermode was selectively excited (solid red line). Spectrum of seed radiation (dashed blue line).

It is important to note that we did not need any permanent active feedback system to selectively excite a supermode in the MCF. After the initial adjustment of the phase mask on the SLM was done, the coupling efficiency of a supermode could decrease only due to mechanical drifts, and we only needed to readjust relative positions of the elements to bring high coupling efficiency back. In our experimental setup, we used the same phase mask on the SLM for several weeks to excite the out-of-phase supermode with equal efficiency. To compensate for drifts, we slightly readjusted (by $\sim 1\text{--}2\ \mu\text{m}$) the position of the input face of the MCF mounted on a three-axis translation stage.

6. Numerical Modeling of Nonlinear Light Propagation

To study the nonlinear regime of light propagation, we performed three-dimensional numerical modeling with allowance for the real geometric structure and refractive index profile of the MCF. The beam propagation modeling was done for continuous-wave light on the basis of a scalar unidirectional wave equation taking into account the refractive index profile and Kerr nonlinearity [36,50]. To achieve the out-of-phase supermode equalization at a reasonable power level, we modeled the MCF with slightly upscaled (by 1.08) sizes of the cores and core-to-core distances. Such a fiber can be manufactured from the same preform by changing the fiber drawing speed. A larger core-to-core spacing leads to a lower coupling coefficient and a lower power required to observe nonlinear mode reshaping, according to Equation (6). In the modeled structure, the individual cores are still single-mode at a wavelength of $1\ \mu\text{m}$. We modeled the propagation of the in-phase and the out-of-phase supermodes with different peak powers over a 20 cm distance. We started our simulations with a low power and used the supermode profiles calculated in the linear regime as initial conditions. We then slowly increased the power and used the output of the previous calculation as an input for the next one. The output profiles of the launched in-phase and out-of-phase supermodes at different power levels are compared in Figure 6. The obtained results clearly show that the in-phase supermode experiences discrete self-focusing and finally collapses into one core. According to the theoretical predictions, the out-of-phase supermode profile at the same power level becomes even flatter. At higher powers, the intensities in all cores become almost equal. No signs of transverse instability were observed for the out-of-phase supermode, which proves its usefulness for high-power light transportation.

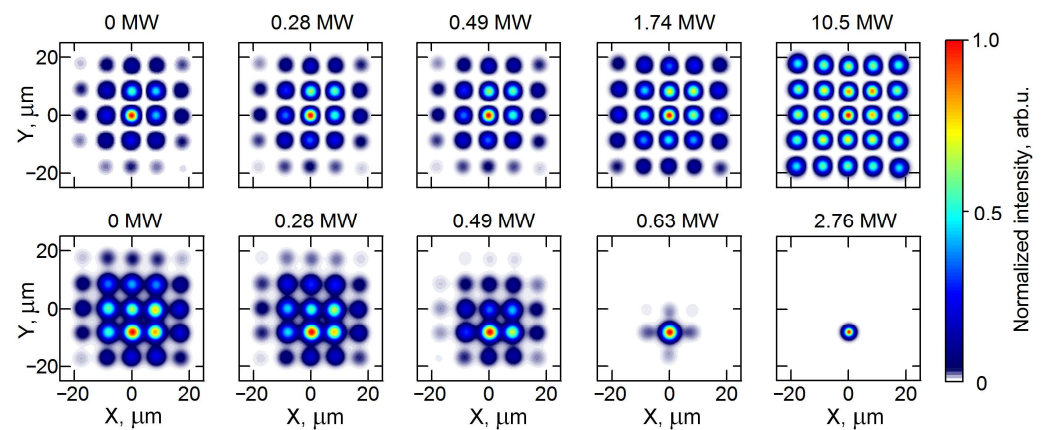


Figure 6. Numerical simulation of the out-of-phase supermode (**upper row**) and the in-phase supermode (**lower row**) propagation at different total power levels.

7. Discussion

The obtained results confirm that in the designed MCF it is possible to selectively excite steadily propagating supermodes, including the out-of-phase supermode. Selective supermode excitation is achieved by using the SLM. The highest out-of-phase supermode is stable and, in principle, can be used for transmitting high power signals, as demonstrated in 3D modeling, whereas the lowest in-phase supermode is unstable and collapses at high powers. These experimental and theoretical studies have demonstrated the great potential of MCFs with coupled cores located at the nodes of a square array for building advanced laser systems.

We did not observe nonlinear mode reshaping in the experiment because our uncompressed pulse laser source did not provide sufficient peak power. The peak power required to observe the out-of-phase mode flattening in the tested MCF estimated on the basis of Equation (6) is above 10 MW, and the corresponding peak intensity is above the material damage threshold. However, we experimentally verified the possibility of selective excitation of supermodes and obtained a good agreement between the measured and numerically calculated mode profiles and group propagation indexes.

The peak power required to observe the supermode profile equalization in the up-scaled fiber in numerical modeling is quite large and may be difficult to achieve in the experiment. However, according to the scaling rule (Equation (6)), in a similar fiber with all the cores separated by a greater distance, the required regime can be observed at significantly lower power levels. Since the evanescent coupling between the cores decreases exponentially with increasing separation between the cores, a 10 times lower coupling coefficient can be achieved by moving the cores farther by only several micrometers. The updated design will be implemented in the next iteration of the MCF manufacturing and experimental testing. We also note that in the telecommunication range at the wavelength of $1.5 \mu\text{m}$ the fiber with a larger diameter of up to $\sim 330 \mu\text{m}$, which can be drawn from the manufactured preform, will have single-mode cores (with a diameter $\sim 10 \mu\text{m}$) and a several times lower coupling coefficient.

8. Conclusions

In this work, we designed and fabricated a silica MCF with 25 coupled cores arranged in a 5×5 square array. We studied the propagation of broadband pulses in this MCF. We created the beam forming system that allowed us to control the power and phase of the signal directed to each core of the MCF. Using this system and an optimization algorithm, we demonstrated the possibility of selective supermode excitation in the fabricated MCF, in particular, the excitation of the in-phase and out-of-phase supermodes. For the first time, we demonstrated coherent propagation of pulses with the content of the out-of-phase supermode reaching 90% in the MCF with a square array of cores. Measured with an inter-

ference method, the phase and intensity distributions of the excited supermodes matched the distributions predicted numerically using the MCF structure. Three-dimensional numerical modeling of nonlinear propagation with allowance for the real geometric structure and refractive index profile of the MCF that can be drawn from the manufactured preform demonstrated stable propagation of the out-of-phase supermode and equalization of the intensities in the cores at high power, as predicted by the theory.

The obtained results confirm that in the designed MCF, where coupled cores are arranged in a square array, it is possible to selectively excite the steadily propagating out-of-phase supermode, which is stable at high power levels. The reported work is an important step toward experimental testing of the possibility of coherent transportation of high-power radiation in multicore fibers.

Author Contributions: Conceptualization, A.V.A. and A.G.L.; methodology, A.V.A., N.A.K., E.A.A., O.N.E. and S.L.S.; software, N.A.K., E.A.A. and A.V.A.; validation, A.V.A. and E.A.A.; formal analysis, A.V.A.; investigation, N.A.K., E.A.A. and A.V.A.; resources, O.N.E., S.G.Z., S.L.S. and A.V.A.; data curation, N.A.K., E.A.A. and A.V.A.; writing—original draft preparation, N.A.K. and A.V.A.; writing—review and editing, E.A.A., N.A.K. and A.V.A.; visualization, N.A.K., E.A.A., O.N.E., S.G.Z. and A.V.A.; supervision, A.V.A. and A.G.L.; project administration, A.V.A. and A.V.K.; funding acquisition, A.V.A. and A.V.K. All authors have read and agreed to the published version of the manuscript.

Funding: This research was supported by the Center of Excellence “Center of Photonics” funded by the Ministry of Science and Higher Education of the Russian Federation, contract No. 075-15-2020-906.

Data Availability Statement: The data presented in this study are available on request from the corresponding author.

Conflicts of Interest: The authors declare no conflict of interest.

References

1. Richardson, D. New optical fibres for high-capacity optical communications. *Phil. Trans. R. Soc. A* **2016**, *374*, 20140441. [[CrossRef](#)]
2. Berdague, S.; Facq, P. Mode division multiplexing in optical fibers. *Appl. Opt.* **1982**, *21*, 1950–1955. [[CrossRef](#)]
3. Ryf, R.; Randel, S.; Gnauck, A.H.; Bolle, C.; Essiambre, R.; Winzer, P.J.; Peckham, D.W.; McCurdy, A.; Lingle, R. Space-division multiplexing over 10 km of three-mode fiber using coherent 6×6 MIMO processing. In Proceedings of the Optical Fiber Communication Conference/National Fiber Optic Engineers Conference, Los Angeles, CA, USA, 6–10 March 2011; p. PDPB10. [[CrossRef](#)]
4. Ryf, R.; Fontaine, N.K.; Chen, H.; Guan, B.; Huang, B.; Esmaelpour, M.; Gnauck, A.H.; Randel, S.; Yoo, S.; Koonen, A.; et al. Mode-multiplexed transmission over conventional graded-index multimode fibers. *Opt. Express* **2015**, *23*, 235–246. [[CrossRef](#)]
5. Lavoute, L.; Roy, P.; Desfarges-Berthelot, A.; Kermene, V.; Fevrier, S. Design of microstructured single-mode fiber combining large mode area and high rare earth ion concentration. *Opt. Express* **2006**, *14*, 2994–2999. [[CrossRef](#)]
6. Wong, W.S.; Peng, X.; McLaughlin, J.M.; Dong, L. Breaking the limit of maximum effective area for robust single-mode propagation in optical fibers. *Opt. Lett.* **2005**, *30*, 2855–2857. [[CrossRef](#)] [[PubMed](#)]
7. Wang, P.; Cooper, L.J.; Sahu, J.K.; Clarkson, W.A. Efficient single-mode operation of a cladding-pumped ytterbium-doped helical-core fiber laser. *Opt. Lett.* **2006**, *31*, 226–228. [[CrossRef](#)]
8. Liu, C.; Chang, G.; Litchinitser, N.; Guertin, D.; Jacobsen, N.; Tankala, K.; Galvanauskas, A. Chirally Coupled Core Fibers at 1550-nm and 1064-nm for Effectively Single-Mode Core Size Scaling. In Proceedings of the 2007 Conference on Lasers and Electro-Optics (CLEO), Baltimore, MD, USA, 6–11 May 2007; pp. 1–2. [[CrossRef](#)]
9. Gaponov, D.A.; Fevrier, S.; Devautour, M.; Roy, P.; Likhachev, M.E.; Aleshkina, S.S.; Salganskii, M.Y.; Yashkov, M.V.; Guryanov, A.N. Management of the high-order mode content in large (40 μm) core photonic bandgap Bragg fiber laser. *Opt. Lett.* **2010**, *35*, 2233–2235. [[CrossRef](#)] [[PubMed](#)]
10. Ramachandran, S.; Nicholson, J.W.; Ghalmi, S.; Yan, M.F.; Wisk, P.; Monberg, E.; Dimarcello, F.V. Light propagation with ultralarge modal areas in optical fibers. *Opt. Lett.* **2006**, *31*, 1797–1799. [[CrossRef](#)]
11. Kaminow, I.; Li, T.; Willner, A.E. *Optical Fiber Telecommunications Volume VII: Systems and Networks*, 6th ed.; Elsevier Science: Oxford, UK, 2013.
12. Willner, A. *Optical Fiber Telecommunications VII*, 1st ed.; Academic Press: London, UK, 2020.
13. Saitoh, K.; Matsuo, S. Multicore Fiber Technology. *J. Lightwave Technol.* **2016**, *34*, 55–66. [[CrossRef](#)]
14. Sano, A.; Takara, H.; Kobayashi, T.; Kawakami, H.; Kishikawa, H.; Nakagawa, T.; Miyamoto, Y.; Abe, Y.; Ono, H.; Shikama, K.; et al. 409-Tb/s + 409-Tb/s crosstalk suppressed bidirectional MCF transmission over 450 km using propagation-direction interleaving. *Opt. Express* **2013**, *21*, 16777–16783. [[CrossRef](#)]

15. Dynes, J.F.; Kindness, S.J.; Tam, S.W.; Plews, A.; Sharpe, A.W.; Lucamarini, M.; Frohlich, B.; Yuan, Z.L.; Pentyl, R.V.; Shields, A.J. Quantum key distribution over multicore fiber. *Opt. Express* **2016**, *24*, 8081–8087. [[CrossRef](#)]
16. Lin, R.; Udalcovs, A.; Ozolins, O.; Pang, X.; Gan, L.; Tang, M.; Fu, S.; Popov, S.; Silva, T.F.D.; Xavier, G.B.; et al. Telecommunication Compatibility Evaluation for Co-existing Quantum Key Distribution in Homogenous Multicore Fiber. *IEEE Access* **2020**, *8*, 78836–78846. [[CrossRef](#)]
17. Ramirez, L.P.; Hanna, M.; Bouwmans, G.; Hamzaoui, H.E.; Bouazaoui, M.; Labat, D.; Delplace, K.; Pouysegur, J.; Guichard, F.; Rigaud, P.; et al. Coherent beam combining with an ultrafast multicore Yb-doped fiber amplifier. *Opt. Express* **2015**, *23*, 5406–5416. [[CrossRef](#)]
18. Klenke, A.; Muller, M.; Stark, H.; Stutzki, F.; Hupel, C.; Schreiber, T.; Tunnermann, A.; Limpert, J. Coherently combined 16-channel multicore fiber laser system. *Opt. Lett.* **2018**, *43*, 1519–1522. [[CrossRef](#)]
19. Lhermite, J.; Suran, E.; Kermene, V.; Louradour, F.; Desfarges-Berthelemot, A.; Barthelemy, A. Coherent combining of 49 laser beams from a multiple core optical fiber by a spatial light modulator. *Opt. Express* **2010**, *18*, 4783–4789. [[CrossRef](#)] [[PubMed](#)]
20. Lin, D.; Carpenter, J.; Feng, Y.; Jain, S.; Jung, Y.; Feng, Y.; Zervas, M.N.; Richardson, D.J. Reconfigurable structured light generation in a multicore fibre amplifier. *Nat. Commun.* **2020**, *11*, 3986. [[CrossRef](#)]
21. Xia, C.; Bai, N.; Ozdur, I.; Zhou, X.; Li, G. Supermodes for optical transmission. *Opt. Express* **2011**, *19*, 16653–16664. [[CrossRef](#)] [[PubMed](#)]
22. Li, H.; Zang, J.; Raghuraman, S.; Chen, S.; Goel, C.; Xia, N.; Ishaaya, A.; Yoo, S. Large-Mode-Area Multicore Yb-Doped Fiber for an Efficient High Power 976 Nm Laser. *Opt. Express* **2021**, *29*, 21992. [[CrossRef](#)]
23. Dostovalov, A.V.; Skvortsov, M.I.; Wolf, A.A.; Labuntsov, V.I.; Egorova, O.N.; Semjonov, S.L.; Babin, S.A. Seven-Core Fibre Raman Laser with Intercore Coupling. *Quantum Electron.* **2020**, *50*, 1088–1090. [[CrossRef](#)]
24. Skvortsov, M.I.; Abdullina, S.R.; Wolf, A.A.; Dostovalov, A.V.; Vlasov, A.A.; Lobach, I.A.; Wabnitz, S.; Babin, S.A. Random Raman Fiber Laser Based on a Twin-Core Fiber with FBGs Inscribed by Femtosecond Radiation. *Opt. Lett.* **2019**, *44*, 295. [[CrossRef](#)] [[PubMed](#)]
25. Chekhovskoy, I.S.; Rubenchik, A.M.; Shtyrina, O.V.; Fedoruk, M.P.; Turitsyn, S.K. Nonlinear combining and compression in multicore fibers. *Phys. Rev. A* **2016**, *94*, 043848. [[CrossRef](#)]
26. Rubenchik, A.M.; Chekhovskoy, I.S.; Fedoruk, M.P.; Shtyrina, O.V.; Turitsyn, S.K. Nonlinear pulse combining and pulse compression in multi-core fibers. *Opt. Lett.* **2015**, *40*, 721–724. [[CrossRef](#)] [[PubMed](#)]
27. Minardi, S.; Eilenberger, F.; Kartashov, Y.V.; Szameit, A.; Ropke, U.; Kobelke, J.; Schuster, K.; Bartelt, H.; Nolte, S.; Torner, L.; et al. Three-Dimensional Light Bullets in Arrays of Waveguides. *Phys. Rev. Lett.* **2010**, *105*, 263901. [[CrossRef](#)]
28. Aceves, A.B.; Shtyrina, O.V.; Rubenchik, A.M.; Fedoruk, M.P.; Turitsyn, S.K. Spatiotemporal optical bullets in two-dimensional fiber arrays and their stability. *Phys. Rev. A* **2015**, *91*, 033810. [[CrossRef](#)]
29. Aceves, A.B.; Angelis, C.D.; Trillo, S.; Wabnitz, S. Storage and steering of self-trapped discrete solitons in nonlinear waveguide arrays. *Opt. Lett.* **1994**, *19*, 332–334. [[CrossRef](#)]
30. Antikainen, A.; Agrawal, G.P. Supercontinuum Generation in Seven-Core Fibers. *J. Opt. Soc. Am. B* **2019**, *36*, 2927. [[CrossRef](#)]
31. Aceves, A.B.; De Angelis, C.; Peschel, T.; Muschall, R.; Lederer, F.; Trillo, S.; Wabnitz, S. Discrete self-trapping, soliton interactions, and beam steering in nonlinear waveguide arrays. *Phys. Rev. E* **1996**, *53*, 1172–1189. [[CrossRef](#)]
32. Andrianov, A.V.; Kalinin, N.A.; Koptev, M.Y.; Egorova, O.N.; Kim, A.V.; Litvak, A.G. High-energy femtosecond pulse shaping, compression, and contrast enhancement using multicore fiber. *Opt. Lett.* **2019**, *44*, 303–306. [[CrossRef](#)]
33. Balakin, A.A.; Skobelev, S.A.; Anashkina, E.A.; Andrianov, A.V.; Litvak, A.G. Coherent propagation of laser beams in a small-sized system of weakly coupled optical light guides. *Phys. Rev. A* **2018**, *98*, 043857. [[CrossRef](#)]
34. Balakin, A.A.; Skobelev, S.A.; Andrianov, A.V.; Anashkina, E.A.; Litvak, A.G. Coherent propagation and amplification of intense laser pulses in hexagonal multicore fibers. *Opt. Lett.* **2020**, *45*, 3224–3227. [[CrossRef](#)]
35. Balakin, A.A.; Litvak, A.G.; Skobelev, S.A. Coherent propagation and amplification of intense wave beams in a deformed multicore fiber. *Phys. Rev. A* **2020**, *102*, 023527. [[CrossRef](#)]
36. Balakin, A.A.; Skobelev, S.A.; Andrianov, A.V.; Anashkina, E.A.; Litvak, A.G. Coherent amplification of high-power laser radiation in multicore fibers from a rectangular array of cores. *Opt. Lett.* **2021**, *46*, 246–249. [[CrossRef](#)] [[PubMed](#)]
37. Tunnermann, H.; Shirakawa, A. Self-focusing in multicore fibers. *Opt. Express* **2015**, *23*, 2436–2445. [[CrossRef](#)]
38. Andrianov, A.V.; Kalinin, N.A.; Anashkina, E.A.; Egorova, O.N.; Lipatov, D.S.; Kim, A.V.; Semjonov, S.L.; Litvak, A.G. Selective Excitation and Amplification of Peak-Power-Scalable Out-of-Phase Supermode in Yb-Doped Multicore Fiber. *J. Lightwave Technol.* **2020**, *38*, 2464–2470. [[CrossRef](#)]
39. Christodoulides, D.N.; Joseph, R.I. Discrete self-focusing in nonlinear arrays of coupled waveguides. *Opt. Lett.* **1988**, *13*, 794–796. [[CrossRef](#)]
40. Andrianov, A.; Kalinin, N.; Anashkina, E.; Leuchs, G. Highly efficient coherent beam combining of tiled aperture arrays using out-of-phase pattern. *Opt. Lett.* **2020**, *45*, 4774–4777. [[CrossRef](#)]
41. Gonda, T.; Imamura, K.; Sugizaki, R. Multicore fiber for bi-directional transmission. In Proceedings of the 2016 21st OptoElectronics and Communications Conference (OECC) Held Jointly with 2016 International Conference on Photonics in Switching (PS), Niigata, Japan, 3–7 July 2016; pp. 1–3.
42. Kobayashi, T.; Nakamura, M.; Hamaoka, F.; Shibahara, K.; Mizuno, T.; Sano, A.; Kawakami, H.; Isoda, A.; Nagatani, M.; Yamazaki, H.; et al. 1-Pb/s (32 SDM/46 WDM/768 Gb/s) C-band Dense SDM Transmission over 205.6-km of Single-mode Heterogeneous

- Multi-core Fiber using 96-Gbaud PDM-16QAM Channels. In Proceedings of the Optical Fiber Communication Conference, Los Angeles, CA, USA, 19–23 March 2017. paper Th5B.1. [\[CrossRef\]](#)
43. Jain, S.; Castro, C.; Jung, Y.; Hayes, J.; Sandoghchi, R.; Mizuno, T.; Sasaki, Y.; Amma, Y.; Miyamoto, Y.; Bohn, M.; et al. 32-core erbium/ytterbium-doped multicore fiber amplifier for next generation space-division multiplexed transmission system. *Opt. Express* **2017**, *25*, 32887–32896. [\[CrossRef\]](#)
 44. Chavez-Pirson, A.; Hwang, B.; Nguyen, D.; Luo, T.; Jiang, S. New approach to image amplification based on an optically pumped multi-core optical fiber. In Proceedings of the SPIE Optics + Photonics, Novel Optical Systems Design and Optimization IX, San Diego, CA, USA, 13–17 August 2006; pp. 67–74. [\[CrossRef\]](#)
 45. Xiong, H.; Gan, J.; Wu, Y. Kuznetsov-Ma Soliton Dynamics Based on the Mechanical Effect of Light. *Phys. Rev. Lett.* **2017**, *119*, 153901. [\[CrossRef\]](#)
 46. Xiong, H.; Wu, Y. Optomechanical Akhmediev Breathers. *Laser Photonics Rev.* **2018**, *12*, 1700305. [\[CrossRef\]](#)
 47. Andrianov, A.; Anashkina, E.; Muravyev, S.; Kim, A. All-fiber design of hybrid Er-doped laser/Yb-doped amplifier system for high-power ultrashort pulse generation. *Opt. Lett.* **2010**, *35*, 3805–3807. [\[CrossRef\]](#)
 48. Bobkov, K.; Andrianov, A.; Koptev, M.; Muravyev, S.; Levchenko, A.; Velmiskin, V.; Aleshkina, S.; Semjonov, S.; Lipatov, D.; Guryanov, A.; et al. Sub-MW peak power diffraction-limited chirped-pulse monolithic Yb-doped tapered fiber amplifier. *Opt. Express* **2017**, *25*, 26958–26972. [\[CrossRef\]](#)
 49. Egorova, O.N.; Astapovich, M.S.; Belkin, M.E.; Semenov, S.L. Fiber-Optic Delay Line Using Multicore Fiber. *Bull. Lebedev Phys. Inst.* **2017**, *44*, 5–7. [\[CrossRef\]](#)
 50. Andrianov, A.; Anashkina, E.; Kim, A.; Meyerov, I.; Lebedev, S.; Sergeev, A.; Mourou, G. Three-dimensional modeling of CPA to the multimillijoule level in tapered Yb-doped fibers for coherent combining systems. *Opt. Express* **2014**, *22*, 28256–28269. [\[CrossRef\]](#)